Design for Nano-Robots Exposing Cancer Cells

by

Shlomi Dolev, Michael Rosenblit and Ram Prasadh Narayanan

Technical Report #18-02

May 08, 2018

The Lynne and William Frankel Center for Computer Science,

Department of Computer Science,

Ben-Gurion University, Beer Sheva, Israel.

Design for Nano-Robots Exposing Cancer Cells

(Preliminary Version)

Shlomi Dolev[1], Michael Rosenblit[2] and Ram Prasadh Narayanan[1]

[1]Department of Computer Science, Ben-Gurion University of the Negev. Email: {dolev,narayan}@cs.bgu.ac.il
[2]Ilse Katz Institute of Nano-Scale Science and Technology, Ben-Gurion University of the Negev. Email: rmichael@bgu.ac.il

May 8, 2018

Abstract

A proof-of-concept design of a nano-robot which can navigate, detect cancer cells and actuate the release of chemicals in blood is discussed. The nano-robot is designed with blood energy harvesting capability and accumulation of electricity in a capacitor, that forms the main body of the nano-robot. The nano-robot is immobilized with glucose hunger-based cancer detectors that reduce the electrical resistance of a nano-tube when attached to a cancer cell. This mechanism, in turn allows electric current to activate a nano-electrical-mechanical (NEM) relay (mechanical transistor) to break the ceiling, exposing a chemical material identified by the immune system for cell elimination. This concept is in line with the effort to design an autonomous computational nano-robot for in-vivo medical diagnosis and treatment. The concept can also be considered as a step to bridge the gap between theoretical swarming/navigation techniques and a computational hardware for plausible implementation of the theory.

1 Introduction

In general, programmable matter is any matter that has the ability to change its physical properties (like shape, density, moduli, conductivity, optical properties, etc.) based on user input or autonomous sensing. We are particularly interested in implementable programmable matter composed of nano-robots. Advances in electronic fabrication satisfies the necessity of resource adequacy in nano computational systems and the implementation feasibility of particle systems make it possible to incorporate nano-computational systems into materials used in paint coating, structural integrity, vibration sensors etc. [1]. Recent advances in controlling mechanisms in biological systems, such as cell signaling, cell movement and nano delivery devices for area focused treatment [2–5], motivate the need for further research in these areas. Models for programmable matter exist in computational geometry [6–10], synthetic biology [11–13], swarm robotics [14–18] and distributed computing [19, 20]. But most of these fields have focused on obtaining theoretical results rather than a possible implementation.

Nano-robotics is a rapidly growing interdisciplinary field addressing the assembly and utilization of molecular devices based on nano-scale principles [21]. Key applications to nano-robotics are medical target identification, targeted drug delivery and minimal invasive surgery [22–24], to name a few. In our previous work [25], we presented a swarming algorithm for *in-vivo* nano-robots,

inspired by caterpillar swarm in nature, wherein the nano-robots were considered as large quantities of programmable matter. We suggested instructing the computational particles to create layered and connected structures for the benefit of speed and energy preservation. We put forward a proposition, that the theoretical concept needs to be supported by hardware feasibility for a plausible implementation of a computational nano-robot. Through this work, we have attempted to design autonomous nano-robots which can harvest energy from the glucose in the blood and activate a response, based on bio-detection. We will present below the design of the nano-robot structure with three modules, (*i*) External coated energy harvester electrodes and cylindrical capacitor, (*ii*) Detector and (*iii*) Actuator. We believe this facile theory of inorganic nano-robot platform design can help to bridge the gap between existing research on bio-nano sensing in combination with advanced nano transistor technology towards cancer treatment. A collective system of electrical manipulation, bio-detection and NEM actuation can visualize the programmability in the nano matters.

2 Design of Nano-Robot Structure

2.1 Energy harvester and Metal-Insulator-Metal (M-I-M) cylindrical nano-capacitor

A nano-robot can be termed autonomous if there is no dependency on external sources for its operation. The first step to visualizing an autonomous nano-robot is to provide an energy source to it. Thus, as a first module, we wanted to show that autonomy can be introduced to the nano-robot by harvesting energy from the blood. In references [26–28], inorganic glucose energy harvesters were fabricated and analyzed for their efficiency. Certain inorganic materials, like platinum, graphene etc., are used as electrodes due to their bio-compatibility and tested usage scenarios [27, 29, 30]. An open circuit voltage, V_{oc} of $192-860\ mV$, was reported from glucose fuel cells in [26, 28]. Next, we detail our estimation of capacitance of a cylindrical capacitor based on properties of blood, in particular, its glucose concentration.

At injection, the nano-robots are under constant influence of the blood. The velocity of blood flow ranges from $0.3-40\ cm/sec$ [31]. The total surface area of the anode in the cylindrical nano-robot is given by

$$\pi r^2 + 2\pi rh = (\pi \times 50^2) + (2\pi \times 50 \times 40)$$
$$= 2.041 \times 10^{-10} cm^2$$

where, $50nm$ and $40nm$ is the radius and height of the anode, respectively. With the displacement of $0.3-40\ cm$, volume of blood interacting with the nano-robot per second is equal to the surface area of the nano-robot multiplied by the blood velocity[1]:

$$(2.041 \times 10^{-10} \times 0.3) \leftrightarrow (2.041 \times 10^{-10} \times 40)$$
$$= (6.123 \leftrightarrow 816.4) \times 10^{-14} L/Sec$$

Glucose concentration in the human blood is $(3.9-6.4)\ mM/L$. On average, if $5.5\ mM/L$ is the concentration of glucose, the number of moles of glucose interacting with the nano-robot is given as the product of concentration of glucose in blood and the volume of blood interacting with the nano-robot, as:

$$\Big((6.123 \times 5.5) \leftrightarrow (816.4 \times 5.5)\Big) \times 10^{-14}$$
$$= (33.67 \leftrightarrow 4490.2) \times 10^{-14} mM/Sec$$

[1]The $\leftrightarrow$ in the equations indicate '*to*', as 'value A *to* value B'

The avagardo's constant is given by 6.023×10^{23}. Thus the number of molecules of glucose in the interacting volume of blood is given as:

$$\Big((33.67 \times 6.023) \leftrightarrow (4490.2 \times 6.023)\Big) \times 10^{-14} \times 10^{23}$$

$$= 20.2 \leftrightarrow 2704.4 \times 10^{10} Molecules$$

As stated in references [26, 28], abiotic glucose oxidation liberates maximum of 2 electrons per glucose molecule. Thus, the number of electrons in the interacting molecules is given by:

$$\big(2 \times (20.2 \leftrightarrow 2704.4) \times 10^{10}\big)$$

$$= (40.4 \leftrightarrow 5408.8) \times 10^{10} Electrons/Sec$$

Thus, the source current of the harvester is calculated to be the product of number of electrons and charge per 1 electron:

$$(40.4 \times 10^{10} \times 1.6 \times 10^{-19}) \leftrightarrow (5408.8 \times 10^{10} \times 1.6 \times 10^{-19})$$

$$= (64.64 \leftrightarrow 8654) nA$$

Maximum charge stored in the capacitor is given by

$$Q_{max} = C/V_{oc}$$

$$C = \frac{\epsilon_0 \epsilon_r A}{d}$$

where A is the surface area of the capacitive plate and d is the thickness of dielectric. The total surface area available for the capacitor is given as:

$$A = 2\pi r_1 h + 2\pi r_2 h + 2\pi r_3 h = 2\pi h(r_1 + r_2 + r_3)$$

$$2\pi \times 80nm(41 + 30 + 19) = 45216nm^2 = 4.52 \times 10^{-14} m^2$$

where, r_1, r_2, r_3 are the radius of concentric cylinders in the capacitor as shown in 1. Thus, the capacitance calculated for the surface area and with quartz dielectric (relative permittivity $\epsilon_r = 4.7$ and conductance $\sigma = 10^{-14} S/m$) is:

$$C = \frac{8.854 \times 10^{-12} \times 4.7 \times 4.52 \times 10^{-14}}{4 \times 10^{-9}} = 4.702 \times 10^{-16} F$$

$$Q_{max} = C/V_{oc} = 2.449 pC$$

The charging time of the capacitor is given by fraction of maximum charge storage to the generated charge per second:

$$\big(2.449 \times 10^{-12}/8654 \times 10^{-9}\big) \leftrightarrow \big(2.449 \times 10^{-12}/64.64 \times 10^{-9}\big)$$

$$= 0.3 \leftrightarrow 38 \mu Sec$$

Variation in charging time is proportional to the velocity of the blood flow and the total surface area of the anode in the cylindrical nano-robot.

To compliment the calculations of the capacitance, we simulated a 3-D model of a concentric cylindrical Metal-Insulator-Metal (M-I-M) encapsulated capacitor using COMSOL Multiphysics (License #17076110). Fig.1 depicts the structure. The capacitor is charged to the open circuit voltage V_{oc}. The height and diameter of the structure was fixed at 100 nm and 90 nm, respectively (a 10 nm thick outer electrode layer is assumed for the energy harvester). Each metal cylinder is

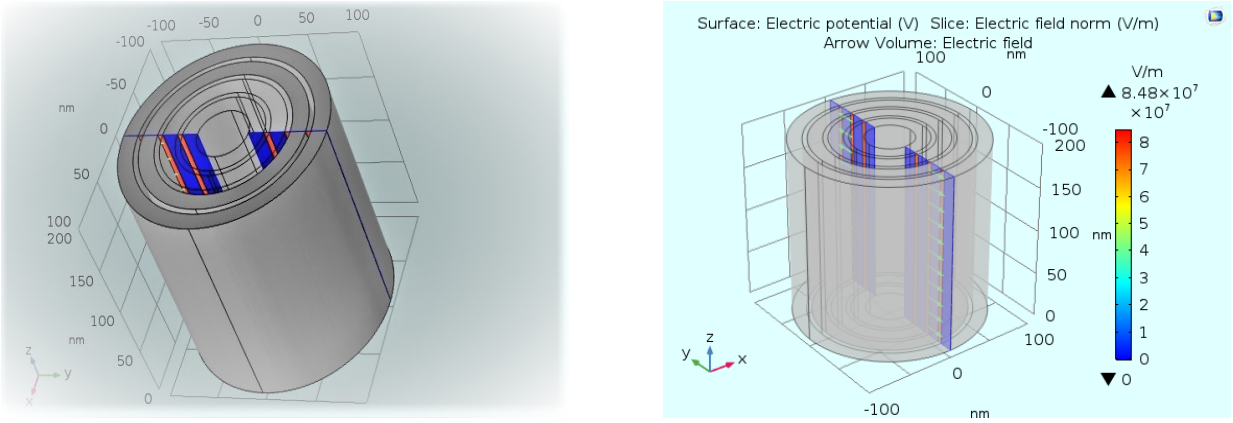

(a) (b)

Figure 1: (a) Structure of concentric cylindrical capacitor (b) The electric field strength in the dielectric and air domain surrounding the capacitor *(green arrows perpendicular to the z-axis)*

10 nm in thickness. Four metal cylinders are arranged concentrically (inside each other) with 4 nm thick dielectric layers separating them. The alternate metal cylinders are imagined extending outside along the vertical axis at the extremes to differentiate positive and negative cylinders connected to respective electrodes of the harvester. This design was chosen to increase the surface area of the capacitor, eventually improving the capacitance. The structure was designed with quartz dielectric ($\epsilon_r = 4.7$ and $\sigma = 10^{-14} S/m$). Appropriate boundary conditions were applied at the interface of air/dielectric in alternate discs. The capacitance of the device was computed to be 4.326×10^{-16} F. Thus, the analyzed and simulated capacitance were nearly equal.

The simulated structure is precisely maintained within a $100nm$ dimension to (i) Qualify the structure as a nano-robot, (ii) To allow the nano-robot to immobilize itself on the cell surface and act as a parasite. The provided energy harvesting capability will enhance the nano-robot to power, in particular, the detector to be used for actuation.

2.2 Bio-Detector

As we mentioned before, a collective system of electrical manipulation, bio-detection and NEM actuation can visualize the programmability in the nano matters. The second part of our proof-of-concept is to show the bio-detection mechanism of cancer cells and to provide an electrical output to logical decisioning. Detection of tumor cells, *in-vivo*, also means the active navigation of the nano-robots using chemical pheromones, acoustic vibrations, photo/fluorophores etc., for binding to tumor tissues. In our case, the glucose hunger of cancer cells and the nano-robots immobilized with glucose or its variants, yield their navigation in blood [32]. Assuming, that our nano-robots can swim randomly in blood, gets attracted to glucose hunger locations, harvest and store energy from the blood glucose. The next step would be to utilize stored charges for a logical decision making. The black-box between harvested energy and decisioning is the mechanism of bio-detection. A chemical detection of cancer cell should induce a change in the charge flow between the electrodes. This hysteresis in charge flow rate can be considered as an electrical normalized low and high. The warburg effect states that cancer cells effectively consume 28% more glucose than normal cells (anaerobic glycolysis) [33]. In our design, we intend to use metallic carbon-nanotubes (CNTs) which are immobilized with variants of glucose, which attaches themselves to the cancer cells by detecting the glucose hunger in cancer cells. In a sense, the nano-robots use glucose hunger and concentration change to *navigate and detect* cancer cells. Fig. 2 shows a schematic of an attached CNT to a cancer cell.

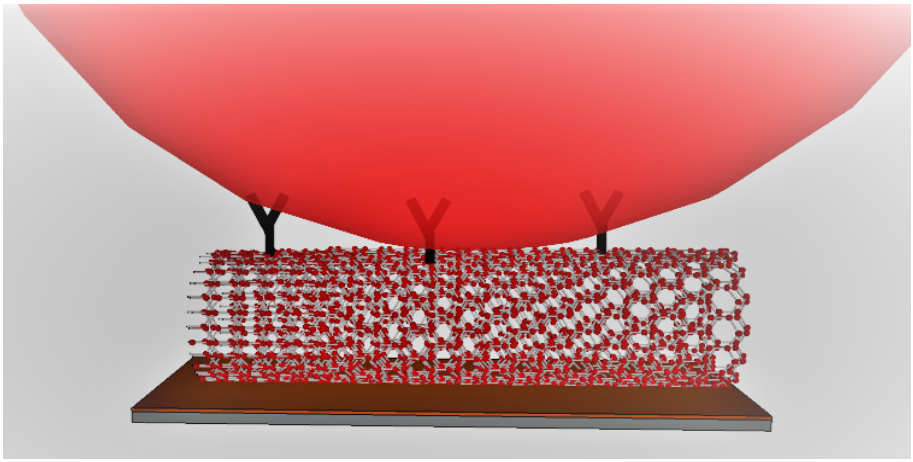

Figure 2: Schematic (not in scale) of a cancer cell attached to a drug supported CNT platform

CNTs can be used as channel materials due to their tunable electrical parameters, mechanical stability, ballistic transport and high current carrying ability. Theoretical calculations and measurements prove that the ballistic transport[2] and mean free path of electron transfer in CNTs extend to over $1\mu m$ [34]. Single walled CNTs (SWCNT) have been tested for their use as bio-detectors. The most important requirement for a CNT bio-sensor is the electrical conductivity of the device as it directly defines the bio-detection capability of the CNTs. Enzyme-coated SWCNTs referred here [35] showed strong pH dependence, wherein the conductance of bare CNTs reduced with glucose immobilization and increased by over 10% when glucose molecules were added to them, suggesting their use for glucose hunger and bio-detection.

The conductance of the immobilized glucose hunger detector before and after detection is given as:

Before glucose hunger detection: $\approx 2.4\ \mu S$

$$R = \frac{1}{2.4\mu S} = 0.42M\Omega$$

After glucose hunger detection: $\approx 2.7\ \mu S$ ($\approx 10\%$ increase)

$$R = \frac{1}{2.7\mu S} = 0.37M\Omega$$

Estimated time constant of the signal (before detection):

$$\tau = RC = 0.42 \times 10^6 \times 4.326 \times 10^{-16} = 182pS(pico)$$

Estimated time constant of the signal (after detection):

$$\tau = RC = 0.37 \times 10^6 \times 4.326 \times 10^{-16} = 160pS(pico)$$

Any capacitor discharges within 5τ [36]. In this case, if V_{oc} is assumed to be $\approx 200mV$, $\approx 1.2\tau$ will be the estimated time until which operable voltage and current is supplied to the actuator, when no current leakage exists. Later, we show that the current leakage implies doubling the time constant values. We tune up the design of the detector so that the change in conductance, before and after immobilization, can be attributed to the capacitance change of the CNT. Likewise, work

[2]Transport of electrons from one end to another without loss of energy inside the medium, i.e, the electrons travel inside the medium as a ballistic missile.

in [37, 38] describes the capture of breast cancer cell lines on CNT arrays. The change in specific conductance of the CNT was considered as the electrical signature for detection of the cancer cells spiked on the blood sample. Different combinations of anti-bodies and cancer cell lines were tested to know the best combination which provides higher conductance change. All the above presented data portrays CNTs as excellent materials for applications demanding higher conductivity, current carrying capacity, ballistic electron transport and bio-detection. We are aware of the quantum effects in CNT devices [39] which would be also considered when the design is elaborated.

2.3 Actuator

Until this stage, the concept is extended to the point where the nano-robots are autonomous in terms of their power and navigation, and computationally equipped to handle a bit change of information. Programmable matters are often imagined to express color changes for swarming, communication and other forms of actuation. In this section, we will discuss the possibility of a Nano-Elecro-Mechanical (NEM) switch which gets triggered by the conductance change of immobilized CNT bio-detector. This will ensure that the matters will respond appropriately depending on the decided logical operation. Miniature mechanical switches suitable for applications, which require less than $100mV$ for operation, were demonstrated here [40, 41]. An MEM actuator switch was demonstrated to operate with a minimum switching voltage of $80mV$[40]. We have already shown in subsection 2.1 that a cylindrical capacitor can harvest sufficient charges to provide an operable voltage of $192 - 860\ mV$. In this section, we show that a mechanical chamber can be designed to lock necessary drug or a combination of drugs, that can be unlocked when increase in electrical power flow due to bio-detection provides adequate electrostatic force to break the ceiling of the chamber, eventually exposing the drug to the environment. This setup can be synonymous to color change or fluorescent marking of a programmable matter. In this regard, we calculated and simulated a NEM actuator which can be broken. Within a unit time constant $\tau = RC$, where R is the resistance and C is the capacitance of the energy harvester, the operating voltage supplied from the energy harvester is expected to drop from $200mV$ to $70mV$. This discharge (until $\approx 1\tau$) can be utilized to provide operable current and voltage for the NEM device actuation. This signal is expected to cause a mechanical break, high enough to surpass the stress gradient of the ceiling structure in the actuator. The mechanical break exposes a detectable drug causing the immune system to recognize the attached nano-robot and the cancer cell. We can also consider the NEM actuator as a parallel plate capacitor. Hence, the electrostatic force F_e acting on the parallel plates due to change in dielectric thickness is given by

$$F_b = F_e = \frac{1}{2} V_b^2 \frac{\epsilon A_c}{d^2} \tag{1}$$

where V_b and F_b are the breakdown voltage and force of the NEM chamber with the glued drug inside it, A_c is the area of the ceiling, and d is the distance between the plates. Fig. 3 shows the circuit schematic and its equivalent sketch of the chamber. The resistances R_1 and R_2 tune the breakdown voltage V_b, such that the NEM chamber collapses. With increase in V_b (due to resistance change after detection), F_e is increased to reach F_b, the force required to trigger a permanent breakage. Before detection, there is leakage of current from the energy harvester to the actuator. Since we consider the actuator as parallel capacitive plates, the capacitance increases in the plates until the capacitor is full. On the other hand, the discharge also happens through the resistor R_2(3b). Thus the value of R_2 has to be maintained, such that, the discharge is lesser than the charging rate and at the same time, the charge-discharge rate of the actuator capacitor is higher and lesser than the charging time of the energy harvester before and after detection, respectively. This ensures that the actuator would not actuate to a false high signal.

An increase in input voltage, V_{in} due to detection, will result in the breakage of NEM box (when V_{in} reaches V_b), thus exposing the glued drug. The drug is glued to keep the target associated with

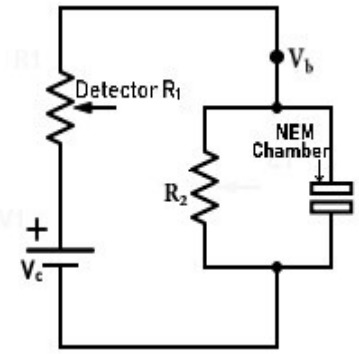

(a)

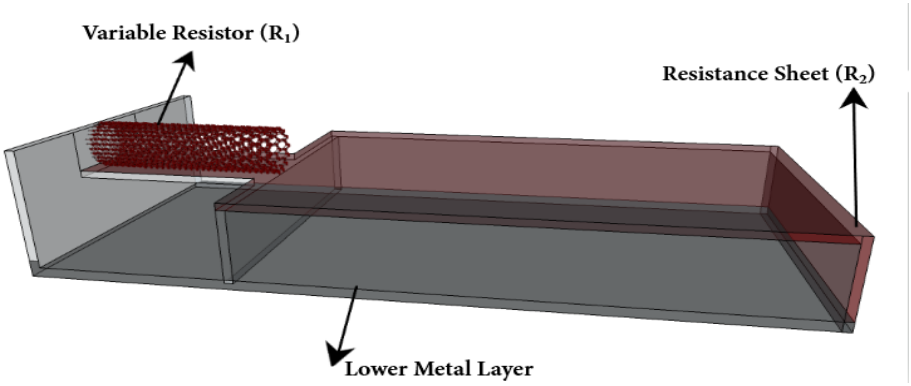

(b)

Figure 3: (a) Circuit schematic for a NEM Actuator (b) Equivalent sketch showing the resistances and the chamber

the cancer cell rather than being distributed in the blood. A sketch and the simulated structure of the actuator is shown in Fig. 4. PMMA polymer material was constructed as the NEM chamber electrode. A non-solid air vacuum was filled as the dielectric. The chamber electrode was fixed at its circumference and simulated. The upper chamber is supported along its outer surface from below. The chamber can be considered as a ceiling, supported along all sides. This design makes sure that the electrostatic force acts uniformly and perpendicular to the chamber surface. Thus the stress on the overall structure is distributed uniformly. The deformation of the PMMA was simulated to be $\approx 0.91nm$ with a maxwell capacitance of 1.5446×10^{-17} F. This deformation distance is approximately equal to the distance between the plates, ensuring a permanent breakage when the breakdown voltage is applied to the plates. The electrostatic force F_e on the chamber electrode was found to be $\approx 1.476nN$.
The selection of NEM actuator material is based on certain parameters like true stress, tensile strength, physical dimensions of the actuator etc. The true stress (σ_t) of the chamber electrode can vary between $\sigma_{t_{min}} \leq \sigma_t \leq \sigma_{t_{max}}$, meaning that F_e can vary between $F_{e_{min}} \leq F_e \leq F_{e_{max}}$. The electrostatic forces $F_{e_{min}}$ and $F_{e_{max}}$ are the minimum and maximum thresholds of force respectively, where $F_{e_{max}} + \Delta F_e$ is the ultimate electrostatic force where a breakage is certain to occur. As an example, true stress value of PMMA polymer ranges from $53.8 \leq \sigma_t \leq 72.4$ [42]. Every single NEM actuator cannot be tested for its true stress. Thus it is presumed that the electrostatic force acting on the chamber surface is smaller than $F_{e_{min}}$, before detection, and higher than $F_{e_{max}}$, after detection, i.e,

Before Detection: $F_s = \frac{1}{2} V_s^2 \frac{\epsilon A_c}{d^2}$, where, $F_s < F_{e_{min}}$ (Stable state)

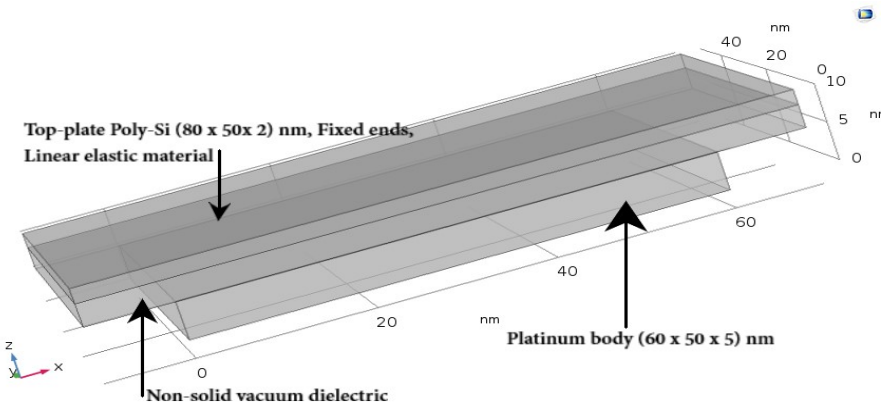

(a)

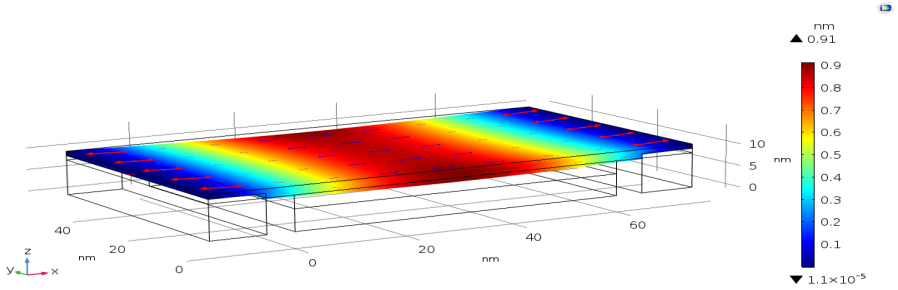

(b)

Figure 4: (a) Sketch of the NEM Actuator as a parallel plate capacitor (b) Displacement of the Poly-Si chamber electrode to $\approx 0.91nm$

After Detection: $F_b = \frac{1}{2}V_b^2\frac{\epsilon A_c}{d^2}$, where, $F_b \geq (F_{e_{max}} + \Delta F_e)$ (Breaking condition)

The electrostatic force, due to the applied voltage is equal to the applied force (due to a load) on the chamber electrode. Therefore, the condition for after detection can be rewritten as

$$\sigma_t \times A_c = \frac{1}{2}V_b^2\frac{\epsilon A_s}{d^2} \tag{2}$$

A_c is the area of the actuator ceiling, given by $2(l + w) \times t_c$, where l and w are the length and width of the chamber electrode, t_c is the thickness of the surface connected to the lower electrode and A_s is the area that suffers from the shear force. As an example, if the chamber electrode is considered to be of (80 x 60 x 2)nm, the thickness t_c is less than the actual thickness elsewhere. This is to make sure that the structure is holded in a fragile manner along its circumference, so as to reduce the force required to collapse the actuator. Thus, substituting it in (2), we get,

$$\sigma_t \times 2(80 + 60) \times t_c = \frac{1}{2}V_b^2\frac{\epsilon \times 80 \times 60}{d^2}$$

The (only) unknown, t_c can be calculated and tuned to the levels of force such that the conditions of F_s and F_b holds true. Substituting the known values of V_b, σ_t, d and ϵ, the thickness of the surface is calculated to be $t_c = 0.35 \leftrightarrow 3$nm.

As an example, substituting $t_c = 0.35nm$ in 2, we get,

$$53.8 \times 2(80 + 60) \times 0.35 \times 10^{-9} = \frac{1}{2} \times \left(V_c^2 \times \left(\frac{R_2}{R_1 + R_2}\right)^2 \times \frac{4.2 \times 80 \times 60}{\left(4 \times 10^{-9}\right)^2}\right)$$

$$15064 \times 0.35 \times 10^{-9} = 2520 \times 10^{-16} \times \left(\frac{R_2}{R_1 + R_2}\right)^2$$

$$\frac{15064 \times 0.35 \times 10^{-9}}{2520 \times 10^{-16}} = \left(\frac{R_2}{R_1 + R_2}\right)^2$$

$$20.92 \times 10^6 = \left(\frac{R_2}{R_1 + R_2}\right)^2$$

$$4.573 \times 10^3 = \left(\frac{R_2}{R_1 + R_2}\right)$$

$$4.573 \times 10^3 \times (R_1 + R_2) = R_2$$

solving which we get R_2 to be $\approx 0.4M\Omega$. Substituting $t_c = 3nm$, we get approximately the same value for R_2.

$$53.8 \times 2(80 + 60) \times 3 \times 10^{-9} = \frac{1}{2} \times \left(V_c^2 \times \left(\frac{R_2}{R_1 + R_2}\right)^2 \times \frac{4.2 \times 80 \times 60}{\left(4 \times 10^{-9}\right)^2}\right)$$

$$15064 \times 3 \times 10^{-9} = 2520 \times 10^{-16} \times \left(\frac{R_2}{R_1 + R_2}\right)^2$$

$$\frac{15064 \times 3 \times 10^{-9}}{2520 \times 10^{-16}} = \left(\frac{R_2}{R_1 + R_2}\right)^2$$

$$179.33 \times 10^6 = \left(\frac{R_2}{R_1 + R_2}\right)^2$$

$$13.39 \times 10^3 = \left(\frac{R_2}{R_1 + R_2}\right)$$

$$13.39 \times 10^3 \times (R_1 + R_2) = R_2$$

solving which, we get R_2 to be $\approx 0.4M\Omega$.

Once the applied voltage reaches V_b, the relay becomes unstable, thus resulting in a permanent breakage. We have also modeled the structure in Fig. 3a for its circuit parameters. The NEM actuator can also be considered as a single shell (the resistor and capacitor) and an external resistor, connected to a supply voltage. The current I_a through the actuator is given by

$$I_a = \frac{V_c}{R_1 + R_2}$$

$$V_b = V_c . \frac{R_2}{R_1 + R_2} = I_a R_2$$

where, V_c is the supply voltage to the actuator, V_b is the breakdown voltage, R_1 is the detector CNT and R_2 is the sheet resistance. The current I_a is given by:

$$I_a = \frac{200mV}{0.42M\Omega} = 0.476\mu A \text{ (before detection)}$$

$$I_a = \frac{200mV}{0.37M\Omega} = 0.540\mu A \text{ (after detection, } \approx 11\% \text{ increase in current flow)}$$

At the same time instance, a current I_l is depleted through R_2, given by:

$$I_l = \frac{V_c}{R_1 + R_2}$$

$$I_l = \frac{200mV}{0.4M\Omega + 0.4M\Omega} = 0.25\mu A$$

The leakage current is lesser than (half) the actuator current which in turn implies doubling the time needed to charge the actuator, i.e, doubling the time estimated in Section 2.2, before and after detection.

3 Conclusion and future work

A facile approach of an energy harvester, glucose hunger detector for cancer cells and actuator for drug exposure design is discussed. A collective system of electrical manipulation, bio-detection and NEM actuation to visualize the programmability in nano-robots is presented. The calculations and simulation results provide a proof-of-concept towards a plausible implementation of an autonomous computational nano-robot with bio-detection, logical decisioning and actuation for drug exposure. To the best of our knowledge, this work is the first of its kind that presents an overall picture towards an autonomous computational nano-robot for cancer diagnosis and treatment.

Acknowledgements

We thank the Lynne and William Frankel Center for Computer Science, the Rita Altura Trust Chair in Computer Science, the Krietman School of Advanced Graduate Studies, Ben-Gurion University of the Negev for their support to this work. We also thank Prof. Zeev Zalevsky from Bar-Ilan University for his useful comments and assistance.

References

[1] H. Abelson, D. Allen, D. Coore, C. Hanson, G. Homsy, Jr. T.F. Knight, R. Nagpal, E. Rauch, G. J. Sussman, and R. Weiss. Amorphous computing. *Commun. ACM*, 43(5):74–82, May 2000.

[2] Wikipedia, cell signaling. `https://en.wikipedia.org/wiki/Cell_signaling`.

[3] R. Ananthakrishnan and A. Ehrlicher. The forces behind cell movement. *International Journal of Biological Sciences*, 3:303–307, 2007.

[4] D. Dolmans, D. Fukumura, and R.K. Jain. Photodynamic therapy for cancer. *Nature Reviews:Cancer*, 3(8):380 – 387, 2003.

[5] S. B. Brown, E. A. Brown, and I. Walker. The present and future role of photodynamic therapy in cancer treatment. *Elsevier, The Lancet Oncology*, 5(8):497 – 508, 2004.

[6] K. C. Cheung, E. D. Demaine, J. R. Bachrach, , and S. Griffith. Programmable assembly with universally foldable strings (moteins). *Trans. Robotics*, 27:718–729, 2011.

[7] C. Moya, X. Doris, and W. Damien. Parallel computation using active self-assembly. *19th International Conference on DNA Computing and Molecular Programming*, pages 16–30, 2013.

[8] E. Demaine and T. Tachi. Origamizer: A practical algorithm for folding any polyhedron. In *In 33rd Intl. Symposium on Computational Geometry*, pages 34:1–34:16, 2017.

[9] Y. J. Chen, B. Groves, R. A. Muscat, and G. Seelig. Dna nanotechnology from the test tube to the cell. *Nature Nanotechnology – Review*, 10:748–760, 2015.

[10] Y. Amir, E. Ben-Ishay, D. Levner, S. Ittah, A. Abu-Horowitz, and I. Bachelet. Universal computing by dna origami robots in a living animal. *Nature Nanotechnology – Letters*, 9:353–357, 2014.

[11] Y. Benenson, T. Paz-Elizur, R. Adar, E. Keinan, Z. Livneh, and E. Shapiro. Programmable and autonomous computing machine made of biomolecules. *Nature*, 414:430–434, 2001.

[12] Ramiz Daniel, Jacob Rubens, Rahul Sarpeshkar, and Tomothy K. Lu. Synthetic analog computation in living cells. *Nature*, 497(7451):619–623, 2013.

[13] Alec A. K. Nielsen, Bryan S. Der, Jonghyeon Shin, Prashant Vaidyanathan, Vanya Paralanov, Elizabeth A. Strychalski, David Ross, Douglas Densmore, and Christopher A. Voigt. Genetic circuit design automation. *Science*, 352(6281), 2016.

[14] P. Flocchini, D. Ilcinkas, A. Pelc, and N. Santoro. Computing without communicating: Ring exploration by asynchronous oblivious robots. *Algorithmica*, 65(3):562–583, 2013.

[15] C. Agathangelou, C. Georgiou, and M. Mavronicolas. A distributed algorithm for gathering many fat mobile robots in the plane. In *Proc. of the 2013 ACM Symp. on Principles of Distributed Computing*, pages 250–259, 2013.

[16] M. Cieliebak, P. Flocchini, G. Prencipe, and N. Santoro. Distributed computing by mobile robots: Gathering. *SIAM Journal on Computing*, 41(4):829–879, 2012.

[17] P. Flocchini, G. Prencipe, N. Santoro, and P. Widmayer. Arbitrary pattern formation by asynchronous, anonymous, oblivious robots. *Theoretical Computer Science*, 407(1):412–447, 2008.

[18] M. Rubenstein, A. Cornejo, and R. Nagpal. Programmable self-assembly in a thousand-robot swarm. *Science*, 345(6198):795–799, 2014.

[19] M. Drees, M. Hüllmann, A. Koutsopoulos, and C. Scheideler. Self-organizing particle systems. In *Proc. of the 26th IEEE Intl. Parallel and Distributed Processing Symposium (IPDPS)*, 2012.

[20] F. Hurtado, E. Molina, S. Ramaswami, and V. Sacristán. Distributed reconfiguration of 2d lattice-based modular robotic systems. *Autonomous Robots*, 38(4):383–413, 2015.

[21] Aristides Requicha. Nanorobots, nems and nanoassembly. *Proceedings of the IEEE*, 91(11):1922–1933, 2003.

[22] Wikipedia. Size of a human cell.

[23] P. Rothemund. Folding dna to create nanoscale shapes and patterns. *Nature*, 440:297–302, 2006.

[24] Carlo Montemagno and George Bachand. Constructing nanomechanical devices powered by biomolecular motors. *Nanotechnology*, 10:225–231, 1999.

[25] S. Dolev, S. Frenkel, M. Rosenblit, R. P. Narayanan, and K. M. Venkateswarlu. In-vivo energy harvesting nano robots. In *2016 IEEE International Conference on the Science of Electrical Engineering (ICSEE)*, pages 1–5, Nov 2016.

[26] B. I. Rapoport, J. T. Kedzierski, and R. Sarpeshkar. A glucose fuel cell for implantable brainmachine interfaces. *PLOS ONE*, 7(6):1–14, 06 2012.

[27] M. Frei, J. Erben, J. Martin, R. Zengerle, and S. Kerzenmacher. Nanofiber-deposited porous platinum enables glucose fuel cell anodes with high current density in body fluids. *Journal of Power Sources*, 362:168 – 173, 2017.

[28] Kiichi Niitsu, Takashi Ando, Atsuki Kobayashi, and Kazuo Nakazato. Enhancement in open-circuit voltage of implantable cmos-compatible glucose fuel cell by improving the anodic catalyst. *Japanese Journal of Applied Physics*, 56(1S):01AH04, 2017.

[29] C. Khler, A. Kloke, A. Drzyzga, R. Zengerle, and S. Kerzenmacher. Fabrication of highly porous platinum electrodes for micro-scale applications bypulsed electrodeposition and dealloying. *Journal of Power Sources*, 242:255 – 263, 2013.

[30] S. Kerzenmacher, U. Krling, T. Metz, R. Zengerle, and F. von Stetten. A potentially implantable glucose fuel cell with raney-platinum film electrodes for improved hydrolytic and oxidative stability. *Journal of Power Sources*, 196(3):1264 – 1272, 2011.

[31] P D Stein and H N Sabbah. Turbulent Blood-Flow in Ascending Aorta of Humans with Normal and Diseased Aortic Valves. *Circulation Research*, 39(1):58–65, 1976.

[32] Sarah nano-particle. `http://www.innovex.co.il/_Uploads/dbsAttachedFiles/NewPhasePresentationframeiNNOVEX2016.pdf`.

[33] Maria V Liberti and Jason W Locasale. The warburg effect: how does it benefit cancer cells? *Trends in biochemical sciences*, 41(3):211–218, 2016.

[34] M. S. Purewal, B. H. Hong, A. Ravi, B. Chandra, J. Hone, and P. Kim. Scaling of resistance and electron mean free path of single-walled carbon nanotubes. *Phys. Rev. Lett.*, 98:186808, May 2007.

[35] Koen Besteman, Jeong O. Lee, Frank G.M. Wiertz, Hendrik A. Heering, and Cees Dekker. Enzyme-coated carbon nanotubes as single-molecule biosensors. *Nano Letters*, 3(6):727–730, 2003.

[36] Capacitor charge/discharge. `https://www.electronics-tutorials.ws/rc/rc_2.html`.

[37] F. Khosravi, P. J. Trainor, C. Lambert, G. Kloecker, E. Wickstrom, S. N. Rai, and B. Panchapakesan. Static micro-array isolation, dynamic time series classification, capture and enumeration of spiked breast cancer cells in blood: the nanotubectc chip. *Nanotechnology*, 27(44):44LT03, 2016.

[38] F. Khosravi, P. Trainor, S. N. Rai, G. Kloecker, E. Wickstrom, and B. Panchapakesan. Label-free capture of breast cancer cells spiked in buffy coats using carbon nanotube antibody micro-arrays. *Nanotechnology*, 27(13):13LT02, 2016.

[39] Kazuyuki Uchida, Susumu Okada, Kenji Shiraishi, and Atsushi Oshiyama. Quantum effects in a double-walled carbon nanotube capacitor. *Physical review B*, 76(15):155436, 2007.

[40] Chuang Qian, Alexis Peschot, Benjamin Osoba, Zhixin Alice Ye, and Tsu Jae King Liu. Sub-100 mV computing with electro-mechanical relays. *IEEE Transactions on Electron Devices*, 64(3):1315–1321, 2017.

[41] B. Osoba, B. Saha, L. Dougherty, J. Edgington, C. Qian, F. Niroui, J. H. Lang, V. Bulovic, J. Wu, and T. J. K. Liu. Sub-50 mv nem relay operation enabled by self-assembled molecular coating. pages 26.8.1–26.8.4, Dec 2016.

[42] Jürg Dual, Gerd Simons, Jürgen Villain, Jacaueline Vollmann, and Christina Weippert. Mechanical Properties of MEMS Structures. *ICEM 12 - 12th International Conference on Experimental Mechanics*, (March):8, 2004.